Quantitative characterization of the $(D_2O)_3$ torsional manifold by terahertz laser spectroscopy and theoretical analysis

Mark R. Viant,[a] Mac G. Brown, Jeff D. Cruzan,[b] and Richard J. Saykally[c]
Department of Chemistry, University of California, Berkeley, California 94720

Michel Geleijns and Ad van der Avoird
Institute of Theoretical Chemistry, NSR-Center, University of Nijmegen, Toernooiveld, 6525 ED Nijmegen, The Netherlands

(Received 26 August 1998; accepted 17 November 1998)

We report the measurement of two new perpendicular $(D_2O)_3$ torsional bands by terahertz laser vibration–rotation–tunneling (VRT) spectroscopy of a planar pulsed supersonic expansion. The first (28.0 cm^{-1}) band corresponds to the $k=\pm 2^l \leftarrow 0$ transition, and is the lowest frequency vibrational spectrum observed for a water cluster. The second (81.8 cm^{-1}) band originates in the first excited torsional state, and has been assigned as $k=3^u \leftarrow \pm 1^l$. An effective three-dimensional Hamiltonian is derived to describe the rotational structure of each torsional state. Degenerate torsional levels with $k=\pm 1$ and $k=\pm 2$ exhibit a Coriolis splitting linear in K implying the presence of vibrational angular momentum, and a second-order splitting from off-diagonal coupling between degenerate sublevels with $+|k|$ and $-|k|$. With this effective Hamiltonian we fit a total of 554 rovibrational transitions in five different bands connecting the lowest nine torsional states, with a rms residual of 1.36 MHz. The data set comprises the two new VRT bands together with the 41.1 cm^{-1} parallel band, the 89.6 cm^{-1} parallel band, and the 98.1 cm^{-1} perpendicular band. This analysis provides a comprehensive characterization of the torsional energy levels in $(D_2O)_3$ up to 100 cm^{-1} above the zero-point energy, and confirms the torsional assignments for all five $(D_2O)_3$ VRT bands observed to date. Moreover, it vindicates the adiabatic separation of the trimer torsional and hydrogen bond stretch/bend vibrational modes which underlies the torsional model. © *1999 American Institute of Physics.* [S0021-9606(99)01108-3]

I. INTRODUCTION

Since the initial studies of the structure and tunneling dynamics in water clusters[1–5] by terahertz laser vibration–rotation–tunneling (VRT) spectroscopy, efforts have been focused primarily on quantifying the nature of their intermolecular vibrations. For the dimer, most of the vibrational states occurring below 150 cm^{-1} have been located and are being thoroughly characterized.[6] Of the twelve degrees of freedom in the trimer, only a few low-lying torsional states had been observed prior to this work.[2,7–11] Similarly, only a fraction of the total number of intermolecular vibrations have been characterized so far for the tetramer,[3,12,13] pentamer,[4,14,15] and hexamer.[5,16] All of these spectra have been observed in the ''torsional band'' (or ''bending band'') region of liquid water.[17]

Theoretical efforts to describe torsion in the water trimer have focused on simplified versions of the intrinsic twelve-dimensional intermolecular dynamics. Specifically, the three hydrogen torsions (essentially rotations about a hydrogen donor bond, see Fig. 1) are investigated on a reduced, three-dimensional, potential energy surface. Two such potential surfaces have been constructed specifically for the water trimer, the modEPEN potential surface by Bürgi *et al.*[18] [also referred to as the Bürgi–Graf–Leutwyler–Klopper (BGLK) potential] and the DD potential surface by van Duijneveldt-van de Rijdt and van Duijneveldt.[19] Both torsional potential energy surfaces have G_6 symmetry, viz. they include all six equivalent structures accessible by flipping hydrogen atoms from one side of the trimer ring to the other. No other motions are considered facile.

All of the spectra recorded in the present work and in previous studies result from transitions within the manifold of torsional states. The flips of the hydrogen atoms are symmetrically equivalent to rotations of the water trimer about the C_3 rotational axis and, therefore, the torsional flipping motion is sometimes referred to as ''pseudorotational.'' One of the questions addressed in the present paper is whether this internal motion of the water trimer generates vibrational angular momentum. Several levels of approximation have been employed in calculations of torsional dynamics of the trimer, ranging from one-dimensional[20] and two-dimensional[21] studies to a three-dimensional calculation on the BGLK potential.[22] Most recently, van der Avoird *et al.*[23,24] have reported a more complete three-dimensional calculation which includes both the overall rotation of the water trimer and the Coriolis coupling of this rotation to the torsional modes, as well as bifurcation (or donor) tunneling.

[a]Present address: Department of Animal Science, University of California, Davis, CA 95616.
[b]Present address: Department of Molecular and Cellular Biology, Harvard University, Cambridge, MA 02138.
[c]Berkeley Miller Research Professor 1997-98. Author to whom all correspondence should be addressed.

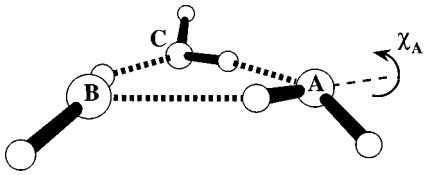

FIG. 1. The *ab initio* equilibrium structure (C_1 symmetry) (Refs. 20 and 25) of $(D_2O)_3$, showing the location of the oxygen atoms (A, B, C) and the bound and free D atoms. Also indicated is one of the three internal rotation angles associated with the torsional or flipping motions of the free D atoms.

The quality of these calculations is naturally limited by the accuracy of the potential energy surfaces used. Furthermore, with only three low frequency torsional bands previously observed and assigned for $(D_2O)_3$ (the 41.1 cm^{-1}, 89.6 cm^{-1}, and 98.1 cm^{-1} bands[9,2,7]), connecting six of the nine lowest lying torsional states, a critical comparison of theory and experiment was hindered. Here we present the observation of two additional VRT torsional transitions at 28.0 and 81.8 cm^{-1}. This permits the characterization of the three remaining low lying torsional states, and enables a global fit of the entire terahertz frequency dataset for $(D_2O)_3$, comprising 554 rovibrational transitions.

II. THEORY

In order to interpret the complex rotational structure in the observed torsional bands, one needs a model Hamiltonian which describes the rotational energy levels for each torsional (or pseudorotational) state. Here we derive such an effective rotational Hamiltonian which takes into account the nonrigidity of the water trimer. In particular, it correctly includes the effects of the Coriolis coupling between the overall rotations of the water trimer and its internal (torsional or ''flipping'') motions.

We start with the Hamiltonian derived in Ref. 23 for the torsional motions of the three monomers in a rotating water trimer

$$H = H^{\mathrm{rot}} + H^{\mathrm{Cor}} + H^{\mathrm{int}}. \tag{1}$$

It was assumed in Ref. 23 that the trimer has a (rigid) cyclic triangular structure, held together by three hydrogen bonds, and that the monomers can only rotate about a single fixed axis. These internal rotations are hindered by a potential which has minima for the external, i.e., nonhydrogen-bonded, protons (or deuterons) lying above or below the plane through the molecular centers of mass. There are six equivalent global minima, and the torsional motions involve ''flips'' of the external protons between these minima. The first term

$$H^{\mathrm{rot}} = B(J_x^2 + J_y^2) + CJ_z^2 \tag{2}$$

is simply the oblate symmetric rotor Hamiltonian for the overall rotation of the complex. The operators J_x, J_y, J_z are the body-fixed components of the total angular momentum operator $\boldsymbol{J}$, depending on the Euler angles describing the orientation of the trimer with respect to a space fixed axis system; B $(=A)$ and C are the rotational constants of $(H_2O)_3$ or $(D_2O)_3$.

The second term

$$H^{\mathrm{Cor}} = -\frac{1}{2}B[(j_+ + j_-^\dagger)J_+ + (j_- + j_+^\dagger)J_-] - C(j_z + j_z^\dagger)J_z \tag{3}$$

represents the Coriolis coupling between the overall angular momentum $\boldsymbol{J}$, with $J_\pm = J_x \mp iJ_y$, and the internal angular momentum $\boldsymbol{j} = \boldsymbol{j}_A + \boldsymbol{j}_B + \boldsymbol{j}_C$ generated by the torsional motions of the monomers *A*, *B*, and *C* about the hydrogen bonds. Explicit expressions for the $\boldsymbol{j}$ components $j_\pm = j_x \pm ij_y$ and j_z in terms of the torsional angles χ_A, χ_B, χ_C are given in Eqs. (A44) and (B5) of Ref. 23. Since these operators are non-Hermitian, Eq. (3) must contain also the Hermitian conjugates $\boldsymbol{j}^\dagger$. In practice, we do not need the explicit form—given in Eq. (A50) of Ref. 23—of these conjugate operators, because in basis set calculations or discrete variable representations (DVR) one can always apply the turn-over rule to replace matrix elements of the Hermitian conjugate operators by the corresponding expressions with the original operators.

The last, internal motion, term in the Hamiltonian

$$H^{\mathrm{int}} = -\frac{\hbar^2}{2\Lambda}\sum_{\nu=A,B,C}\frac{\partial^2}{\partial\chi_\nu^2} + \frac{1}{2}B(j_+^\dagger j_+ + j_-^\dagger j_-) + Cj_z^\dagger j_z + V(\chi_A, \chi_B, \chi_C) \tag{4}$$

describes the torsional motions, with the (model) potential $V(\chi_A, \chi_B, \chi_C)$ defined by fixing all other internal coordinates of the trimer. This model is justified for the ground vibrational state of the hydrogen bonded ''framework'', since the hydrogen bond stretch/bend vibrations have considerably higher frequencies than the torsional motions,[20,25] but it might break down at higher energies. The constant Λ—see Eq. (3) of Ref. 23—in the first kinetic energy term of Eq. (4) is the moment of inertia of each monomer about its fixed axis of rotation, while the remaining kinetic energy terms contain the components of the torsional angular momentum $\boldsymbol{j}$ and their Hermitian conjugates.

In Ref. 24 the complete Hamiltonian of Eq. (1) was used in quantitative DVR calculations of the torsional energy levels for total angular momentum $J=0$, 1 and 2. In the present paper we use this Hamiltonian to derive an effective rotational Hamiltonian for each torsional state, but we also show the results of DVR calculations for $J=0$, 1, 2, and 3 in order to demonstrate that our effective rotational Hamiltonian indeed represents the rotational and Coriolis splittings correctly.

A. Effective rotational Hamiltonian

In various textbooks[26–29] it is shown how an effective rotational Hamiltonian for each vibrational state of a molecule can be derived with the help of Van Vleck perturbation theory. This same formalism has been used[30] to obtain the effective rotor Hamiltonian for each torsional state in a molecule with a single internal rotation. Application of Van Vleck perturbation theory to the water trimer, with the perturbation H^{Cor} included to second order, yields the effective rotational Hamiltonian for torsional state n (an eigenstate of H^{int})

$$H^{\mathrm{rot}}_{\mathrm{eff}(n)} = \langle n|H^{\mathrm{rot}}|n\rangle + \sum_{n' \neq n} \frac{\langle n|H^{\mathrm{Cor}}|n'\rangle\langle n'|H^{\mathrm{Cor}}|n\rangle}{E_n - E_{n'}}, \quad (5)$$

where n' runs over all other eigenstates of H^{int}. Substitution of Eqs. (2) and (3) for H^{rot} and H^{Cor} then gives the effective rotational Hamiltonian

$$H^{\mathrm{rot}}_{\mathrm{eff}(n)} = B(J_x^2 + J_y^2) + CJ_z^2 + \sum_{\alpha,\beta} \mu^{(n)}_{\alpha\beta} J_\alpha J_\beta, \quad (6)$$

where the components α, β run over $+$, $-$, and z. Further,

$$\mu^{(n)}_{++} = \frac{B^2}{4} \sum_{n' \neq n} \frac{\langle n|j_+ + j_-^\dagger|n'\rangle\langle n'|j_+ + j_-^\dagger|n\rangle}{E_n - E_{n'}},$$
$$\mu^{(n)}_{+-} = \frac{B^2}{4} \sum_{n' \neq n} \frac{\langle n|j_+ + j_-^\dagger|n'\rangle\langle n'|j_- + j_+^\dagger|n\rangle}{E_n - E_{n'}}, \quad (7)$$

etc. Actually, since the inverse inertia tensor of the water trimer contains a small ($\approx 1\%$) contribution that depends on the angles χ_A, χ_B, χ_C (see Ref. 23), which must be averaged over the torsional eigenstates $|n\rangle$, the rotational constants B and C are slightly dependent on n.

Since the torsional motions involve ''flips'' between six equivalent minima on the reduced potential surface $V(\chi_A, \chi_B, \chi_C)$, the permutation-inversion (PI) symmetry group of the system is the cyclic group G_6 (isomorphic to the point group C_{3h}), see Ref. 23. From the symmetry of the torsional (pseudorotation) states it follows that many of the matrix elements occurring in Eq. (7) must vanish. These states, denoted from here on by $|k,n\rangle$, can be labeled with the quantum number $k = 0, \pm 1, \pm 2$, or 3 (modulo 6) which corresponds to the one-dimensional complex irreducible representations (irreps) of the group G_6. The index n runs over different states with the same irrep label k. In several papers on the water trimer, including the present one, the ''lower'' levels, with $n = 1$, are denoted by k^l and the ''upper'' levels, with $n = 2$, are denoted by k^u. States with $k = 0$ and $k = 3$ are nondegenerate, states with $k = \pm 1$ and $k = \pm 2$ are twofold degenerate. Wave functions with $k = +1$ and -1 that belong to the same energy are complex conjugate, just as are those with $k = +2$ and -2. In Ref. 23 the following rules were derived.

(i) The operator $j_z + j_z^\dagger$ only couples states with the same quantum number k. Since diagonal matrix elements of j_z are pure imaginary, it follows that the diagonal elements $\langle k,n|j_z + j_z^\dagger|k,n\rangle$ equal zero. Hence, it was concluded that the torsional states do not carry vibrational angular momentum about the z axis (the c axis of the trimer). This holds for any k, including the degenerate levels with $k = \pm 1$ and $k = \pm 2$. Off-diagonal elements $\langle k,n'|j_z + j_z^\dagger|k,n\rangle$ are not necessarily zero.

(ii) The components of $\boldsymbol{j}$ do not obey the commutation relations of ''normal'' angular momentum operators; yet, the operators $j_\pm$ do act as group theoretical shift operators. As a result, the only nonvanishing matrix elements are $\langle k+1,n'|j_+ + j_-^\dagger|k,n\rangle$ and $\langle k-1,n'|j_- + j_+^\dagger|k,n\rangle$.

From rules (i) and (ii) it follows that only the terms with $\mu^{(k,n)}_{++}$, $\mu^{(k,n)}_{+-}$, $\mu^{(k,n)}_{-+}$, $\mu^{(k,n)}_{--}$, and $\mu^{(k,n)}_{zz}$ occur in Eq. (6).

B. Nondegenerate levels $|k,n\rangle$ with $k = 0$ or 3 (modulo 6)

By application of rule (ii) for the matrix elements of the shift operators $j_\pm + j_\mp^\dagger$ it is easily shown that $\mu^{(k,n)}_{++}$ and $\mu^{(k,n)}_{--}$ must vanish. Moreover, we find from the properties of the wave functions and of the shift operators, see Ref. 23, that

$$\langle k' = +1,n'|j_+ + j_-^\dagger|k = 0,n\rangle = -\langle k' = -1,n'|j_- + j_+^\dagger|k = 0,n\rangle^*$$

and

$$\langle k' = -2,n'|j_+ + j_-^\dagger|k = 3,n\rangle = -\langle k' = +2,n'|j_- + j_+^\dagger|k = 3,n\rangle^*$$

and, hence, that $\mu^{(k,n)}_{+-} = \mu^{(k,n)}_{-+}$. Substitution of these results into Eq. (6) yields

$$H^{\mathrm{rot}(k)}_{\mathrm{eff}(n)} = B(J_x^2 + J_y^2) + CJ_z^2 + \mu^{(k,n)}_{+-}(J_+J_- + J_-J_+) + \mu^{(k,n)}_{zz} J_z^2 = [B + 2\mu^{(k,n)}_{+-}](J_x^2 + J_y^2) + [C + \mu^{(k,n)}_{zz}]J_z^2. \quad (8)$$

Effectively, this implies that for the nondegenerate states $|k,n\rangle$ with $k = 0$ and $k = 3$ the rotational constants are changed, but only slightly, from B and C to $B^{(k,n)} = B + 2\mu^{(k,n)}_{+-}$ and $C^{(k,n)} = C + \mu^{(k,n)}_{zz}$.

C. Degenerate levels $|k,n\rangle$ with $k \pm 1$ or $k = \pm 2$ (modulo 6)

Here we must use perturbation theory for degenerate states, i.e., we have to diagonalize the perturbation matrix over the (twofold) degenerate torsional substates. For the levels with $k = \pm 1$ the following terms are nonzero:

$$\mu^{(1,n)}_{+-} = \frac{B^2}{4} \sum_{\substack{n' \\ (k'=0)}} \frac{\langle k=1,n|j_+ + j_-^\dagger|k',n'\rangle\langle k',n'|j_- + j_+^\dagger|k=1,n\rangle}{E_{|k|,n} - E_{|k'|,n'}},$$
$$\mu^{(1,n)}_{-+} = \frac{B^2}{4} \sum_{\substack{n' \\ (k'=2)}} \frac{\langle k=1,n|j_- + j_+^\dagger|k',n'\rangle\langle k',n'|j_+ + j_-^\dagger|k=1,n\rangle}{E_{|k|,n} - E_{|k'|,n'}}, \quad (9)$$

$$\mu_{zz}^{(1,n)} = C^2 \sum_{\substack{n' \\ (k'=1)}} \frac{\langle k=1,n|j_z+j_z^\dagger|k',n'\rangle\langle k',n'|j_z+j_z^\dagger|k=1,n\rangle}{E_{|k|,n}-E_{|k'|,n'}},$$

$$\mu_{++}^{(-1,n)} = \frac{B^2}{4} \sum_{\substack{n' \\ (k'=0)}} \frac{\langle k=1,n|j_+ + j_-^\dagger|k',n'\rangle\langle k',n'|j_+ + j_-^\dagger|k=-1,n\rangle}{E_{|k|,n}-E_{|k'|,n'}}.$$

From symmetry it follows that

$$\begin{aligned} \mu_{+-}^{(-1,n)} &= \mu_{-+}^{(1,n)}, \\ \mu_{-+}^{(-1,n)} &= \mu_{+-}^{(1,n)}, \\ \mu_{zz}^{(-1,n)} &= \mu_{zz}^{(1,n)}, \\ \mu_{--}^{(1,n)} &= [\mu_{++}^{(-1,n)}]^*. \end{aligned} \tag{10}$$

Similarly, for the levels with $k=\pm 2$ the only nonvanishing terms are

$$\begin{aligned} \mu_{+-}^{(2,n)} &= \mu_{-+}^{(-2,n)}, \\ \mu_{-+}^{(2,n)} &= \mu_{+-}^{(-2,n)}, \\ \mu_{zz}^{(2,n)} &= \mu_{zz}^{(-2,n)}, \\ \mu_{--}^{(-2,n)} &= [\mu_{++}^{(2,n)}]^*. \end{aligned} \tag{11}$$

Note that $\mu_{+-}^{(k,n)} \neq \mu_{-+}^{(k,n)}$.

Substitution of these results into Eq. (6) gives

$$\begin{aligned} H_{\mathrm{eff}(n)}^{\mathrm{rot}(k',k)} = \delta_{k',k}[&B(J_x^2+J_y^2)+CJ_z^2+\mu_{+-}^{(k,n)}J_+J_- \\ &+\mu_{-+}^{(k,n)}J_-J_+ + \mu_{zz}^{(k,n)}J_z^2] \\ &+\delta_{k',k-2\ (\mathrm{modulo}\ 6)}\,\mu_{--}^{(k,n)}J_-J_- \\ &+\delta_{k',k+2\ (\mathrm{modulo}\ 6)}\,\mu_{++}^{(k,n)}J_+J_+. \end{aligned} \tag{12}$$

The terms with J_+J_- and J_-J_+, which have unequal coefficients, can be rewritten in terms of $J_+J_-+J_-J_+=2(J_x^2+J_y^2)$ and $J_+J_--J_-J_+=2J_z$, and the effective rotational Hamiltonian becomes

$$\begin{aligned} H_{\mathrm{eff}(n)}^{\mathrm{rot}(k',k)} = \delta_{k',k}[&B^{(|k|,n)}(J_x^2+J_y^2)+C^{(|k|,n)}J_z^2] \\ &\pm\delta_{k',k}[\mu_{+-}^{(|k|,n)}-\mu_{-+}^{(|k|,n)}]J_z \\ &+\delta_{k',k-2\ (\mathrm{modulo}\ 6)}\,\mu_{--}^{(k,n)}J_-J_- \\ &+\delta_{k',k+2\ (\mathrm{modulo}\ 6)}\,\mu_{++}^{(k,n)}J_+J_+ \end{aligned} \tag{13}$$

with the modified rotational constants $B^{(|k|,n)}=B+\mu_{+-}^{(|k|,n)}+\mu_{-+}^{(|k|,n)}$ and $C^{(|k|,n)}=C+\mu_{zz}^{(|k|,n)}$.

The first, rather surprising, observation is the occurrence of a linear Coriolis term, the second term in Eq. (13), which is proportional to J_z although it actually originates from second-order Coriolis coupling. The sign of this term is minus for $k=-1$ or $k=+2$, and plus for $k=+1$ or $k=-2$. This follows directly from the first two lines of Eqs. (10) and (11). Such a linear Coriolis term is usually[27,28] represented in the rotational Hamiltonian by $\mp 2\zeta CJ_z$; in the present case we find that $-2\zeta^{(|k|,n)}C^{(|k|,n)}=\mu_{+-}^{(|k|,n)}-\mu_{-+}^{(|k|,n)}$. Normally the occurrence of such linear terms implies that at least one component of the vibrational angular momentum of some degenerate vibration must have a nonzero expectation value. In this case, however, the expectation value of the corresponding vibrational angular momentum operator $j_z+j_z^\dagger$ vanishes—see point (i) above—and the linear Coriolis term originates purely from second-order perturbation theory. A similar effect was found in earlier work on benzene–Ar,[31,32] where the degenerate van der Waals bending mode carries first-order vibrational angular momentum, but also a substantial second-order contribution. In light of the standard theory for ''normal'' semirigid molecules[27,28] this seems a strange phenomenon, but one should remember that the vibrational angular momentum for such molecules—which perform small amplitude vibrations about a single equilibrium structure—is defined with respect to a body-fixed frame fixed by the Eckart conditions. This choice minimizes the Coriolis coupling between the vibrations and rotations. For the water trimer it does not make sense to define such a frame, because the torsional motions involve tunneling flips between six equivalent equilibrium structures. In the benzene–Ar work[31,32] the body-fixed frame was fixed by the Eckart conditions for the benzene monomer, not by those for the dimer. The occurrence of large second-order contributions to the linear Coriolis term is related to the choice of the body-fixed frame in these systems.

A second observation is the occurrence of J_-J_- and J_+J_+ terms in the effective rotational Hamiltonian. Normally such terms appear for asymmetric rotors with $B\neq A$. Here, these terms are caused by second-order Coriolis coupling, and they occur only for the degenerate levels with $k=\pm 1$ and ± 2. It should be emphasized that they appear in the off-diagonal blocks of the effective rotational Hamiltonian which couple the degenerate substates with $k'=-k$. These substates satisfy the relation $k'=k\pm 2$ (modulo 6), cf. Eq. (13), and, since the shift operators J_-J_- and J_+J_+ couple rotational states with $K'=K-2$ and $K'=K+2$, respectively, the G_6 symmetry rule $k'-K'=k-K$ for the rovibrational states with $J>0$, see Ref. 23, is indeed obeyed.

D. Rotational energy levels

For nondegenerate torsional states with $k=0$ or $k=3$ the effective rotational Hamiltonian is given by Eq. (8) and the rotational levels are simply $B^{(k,n)}J(J+1)+[C^{(k,n)}-B^{(k,n)}]K^2$, where K is the eigenvalue of J_z. For degenerate levels with $k=\pm 1$ or $k=\pm 2$ the effective rotational Hamiltonian given by Eq. (13) should be diagonalized in a basis $|\pm|k|,J,K,M\rangle$. Since the exact quantum number J and its

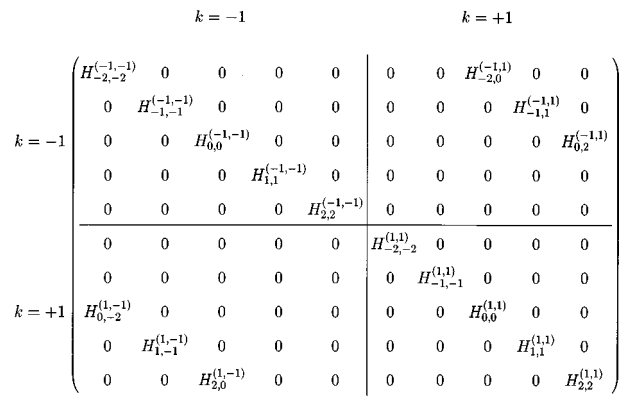

FIG. 2. Effective rotational Hamiltonian matrix for a degenerate level with $k=\pm1$ and $J=2$, with $K=-2,-1,0,1,2$. The diagonal elements are $H^{(\pm1,\pm1)}_{K,K}=B^{(1,n)}J(J+1)+[C^{(1,n)}-B^{(1,n)}]K^2\mp2\zeta^{(1,n)}C^{(1,n)}K$, and the off-diagonal elements are $H^{(1,-1)}_{K+2,K}=[H^{(-1,1)}_{K,K+2}]^*=\mu^{(-1,n)}_{++}[J(J+1)-K(K+1)]^{1/2}[J(J+1)-(K+1)(K+2)]^{1/2}$.

space-fixed z-component M can be given fixed values, it is only K that runs from $-J$ to J and the matrix which must be diagonalized to obtain the rotational levels has dimension $2(2J+1)$. The structure of this matrix follows easily from Eq. (13); it is illustrated in Fig. 2 for a $(k=\pm1,n)$ state with $J=2$. The diagonal elements are $H^{(\pm1,\pm1)}_{K,K}=B^{(1,n)}J(J+1)+[C^{(1,n)}-B^{(1,n)}]K^2\mp2\zeta^{(1,n)}C^{(1,n)}K$, with the linear Coriolis splitting parameter $-2\zeta^{(1,n)}C^{(1,n)}=\mu^{(1,n)}_{+-}-\mu^{(1,n)}_{-+}$ as before. The off-diagonal elements are $H^{(1,-1)}_{K+2,K}=[H^{(-1,1)}_{K,K+2}]^*=\mu^{(-1,n)}_{++}[J(J+1)-K(K+1)]^{1/2}[J(J+1)-(K+1)(K+2)]^{1/2}$. The fact that these off-diagonal matrix elements occur only in the blocks with $k'=-k$ greatly simplifies the calculation of the eigenvalues. Four of the eigenvalues are given directly by diagonal matrix elements, the others are obtained by solving 2×2 problems, i.e., quadratic equations, see Fig. 2. This is in contrast with the asymmetric rotor, where similar off-diagonal matrix elements with $K'=K\pm2$ couple all even and all odd K states. It is very easy to build this calculation of the rotational levels into a fitting program that analyzes the rotational structure of the torsional (or pseudorotational) bands. The linear Coriolis splitting parameter $\zeta=-(\mu_{+-}-\mu_{-+})/(2C)$ and (the absolute value of) the coupling parameter $\mu_{++}=\mu^*_{--}$ of each degenerate state (k,n) with $k=\pm1$ or $k=\pm2$ should then be treated as fit parameters, just as the rotational constants B and C.

III. CALCULATIONS

The rotational and Coriolis splittings of the torsional energy levels can also be deduced from quantitative calculations for $J=0$, 1, 2, and 3 with the complete Hamiltonian of Eq. (1). The DVR method applied in these calculations is described in Ref. 24, the potential $V(\chi_A,\chi_B,\chi_C)$ is taken from *ab initio* calculations by van Duijneveldt *et al.*[19,33] For the (vibrationally averaged) trimer rotational constants we took the values $A=B=0.193\,34\ \mathrm{cm}^{-1}=5796.2$ MHz, $C=0.103\,02\ \mathrm{cm}^{-1}=3088.5$ MHz that have been determined experimentally[7] for the ground state of $(D_2O)_3$. The monomer angle φ_A (see Fig. 1 of Ref. 23) is 58.26° and the rotational constant $\hbar^2/(2\Lambda)$ for the fixed axis rotation of the D_2O monomers is 11.72 cm^{-1}. The angle ξ_A which defines the orientation of the monomer rotation axes with respect to the trimer frame was taken to be 130°. For the overall rotations we used a basis of normalized symmetric top functions $|JKM\rangle=[(2J+1)/8\pi^2]^{1/2}D^{(J)}_{MK}(\alpha,\beta,\gamma)^*$ with fixed J and M, and $K=-J,-J+1,\ldots,J$. The internal coordinates χ_A,χ_B,χ_C are described by the sinc-function DVR of Refs. 34 and 35, with grid boundaries at $\pm112°$ and spacing $\Delta=16°$. The calculations were performed in two steps: in the first step we diagonalized H^{int} in the G_6 symmetry-adapted DVR product basis, in the second step we diagonalized the complete Hamiltonian including H^{rot} and H^{Cor} in a basis of 60 eigenstates from the first step, the lowest 10 eigenfunctions of each symmetry. The results are given in Table I.

TABLE I. Energy levels (in cm^{-1}) of $(D_2O)_3$ from DVR calculations with the complete Hamiltonian and the DD potential of van Duijneveldt *et al.* (Refs. 19 and 33).

Level	k	K	$k-K$	$J=0$	$J=1$	$J=2$	$J=3$
1	0	±3	3				1.4911
		±2	∓2			0.7882	1.9180
		±1	∓1		0.2912	1.0444	2.1741
		0	0	0.0000	0.3766	1.1298	2.2595
2,3	±1	±3	∓2				9.1575
		∓3	∓2				9.1803
		∓2	3			8.4584	9.5883
		∓2	3			8.4584	9.5883
		±2	∓1			8.4736	9.6034
		∓1	±2		7.9652	8.7184	9.8482
		±1	0		7.9726	8.7253	9.8545
		±1	0		7.9730	8.7266	9.8571
		0	±1	7.6778	8.0544	8.8076	9.9374
4,5	±2	±3	∓1				26.6519
		∓3	∓1				26.6856
		∓2	∓2			25.9547	27.0846
		±2	0			25.9771	27.1071
		±2	0			25.9771	27.1071
		∓1	3		25.4632	26.2164	27.3461
		∓1	3		25.4634	26.2168	27.3469
		±1	±1		25.4745	26.2278	27.3577
		0	±2	25.1777	25.5543	26.3076	27.4375
6	3	±3	0				38.1035
		±2	±1			37.4007	38.5307
		±1	±2		36.9037	37.6570	38.7870
		0	3	36.6124	36.9891	37.7424	38.8725

In the $J>0$ energy levels of the states with $k=0$ and $k=3$ one simply observes symmetric rotor splittings. The $J>0$ levels of the degenerate states with $k=\pm1$ and $k=\pm2$ are more interesting because, in addition to the symmetric rotor splittings, one can clearly identify the Coriolis splittings linear in K (and independent of J) between levels with the same $|k|$ and $|K|$, but different $k-K$. From these splittings we derive that $2\zeta^{(|k|,n)}C^{(|k|,n)}$ is $-0.0038\ \mathrm{cm}^{-1}=-114$ MHz for the lowest state with $k=\pm1$ and $-0.0056\ \mathrm{cm}^{-1}=-168$ MHz for the lowest $k=\pm2$ state. Hence, the values of $\zeta^{(|k|,n)}$ for these states are -0.0185 and -0.0272, respectively. One can also observe, for $K=\pm1$, the smaller second-order Coriolis splittings between the two levels with $k-K=0$ for $k=\pm1$ and between the two levels

with $k-K=3$ for $k=\pm 2$. These splittings increase proportionally to $J(J+1)$ with the proportionality constants $2\mu_{++}^{(-1,n)}$ and $2\mu_{++}^{(2,n)}$. For $|K|$ values larger than 1, the latter splittings occur in higher order and have become smaller than 10^{-4} cm^{-1} (which is the precision to which the numbers in Table I have been rounded).

An alternative route that we have followed is the computation of the values of $\mu_{+-}^{(1,n)}$, $\mu_{-+}^{(1,n)}$, $\mu_{zz}^{(1,n)}$, and $\mu_{++}^{(-1,n)}$ and the corresponding parameters for $k=\pm 2$ directly from Eq. (9) with the eigenfunctions $|k,n\rangle$ of H^{int}. Here we also included the lowest 10 eigenstates of each symmetry. The values thus obtained are $\zeta^{(1,n)}=-[\mu_{+-}^{(1,n)}-\mu_{-+}^{(1,n)}]/[2C^{(1,n)}]=-0.0189$ for the lowest state with $k=\pm 1$ and $\zeta^{(2,n)}=-0.0282$ for the lowest $k=\pm 2$ state, in good agreement with the values extracted from the rovibrational levels in Table I. For $\mu_{++}^{(-1,n)}$ and $\mu_{++}^{(2,n)}$ we find complex numbers; their absolute values are 0.000 108 cm^{-1}=3.24 MHz and 0.000 024 cm^{-1}=0.72 MHz, respectively. Knowing the parameter values in the effective rotational Hamiltonian of Eq. (13), we then compute the rotational levels for a given value of J as the eigenvalues of the $2(2J+1)$ dimensional Hamiltonian matrix, see Fig. 2. These levels agree well with those in Table I, which confirms that we have indeed derived a very useful effective rotational Hamiltonian.

IV. MEASUREMENT OF 28.0 AND 81.8 cm^{-1} VRT BANDS

A. Experiment

Both the Berkeley terahertz laser spectrometers[36,37] and the slit jet assembly[38] have been described in detail elsewhere. Hence, only a brief summary of the experiment will be presented here. A high power (100 W), line tunable, infrared CO_2 laser coaxially pumps a fixed frequency far-infrared (FIR) molecular gas laser, the output of which is coupled onto a Schottky barrier diode. The lasers used for the work described here lie at 787.7555 GHz (DCOOD), 849.8280 GHz (HCOOD), 939.4940 GHz (CH_3OD), 2409.2932 GHz (CH_2DOH), 2447.9685 GHz (CH_2F_2), and 2522.7815 GHz (CH_3OH). Tunable coherent FIR light is generated by first-order mixing of the fixed frequency FIR laser radiation with tunable microwave radiation from a HP8673B synthesizer, producing sidebands at frequencies $\nu_{\text{FIR}}\pm n\nu_{\text{MW}}$. The sidebands are then separated from the carrier with a polarizing interferometer and multipassed 22 times through a pulsed planar supersonic expansion before impinging on either an InSb hot electron bolometer (for the low frequency study) or a Ge:Ga stressed photoconductor (for the high frequency study); the multipass cell is arranged in a Herriott configuration.[39] Transient absorption signals measured by the FIR detector are first preamplified and bandpass filtered (SRS SR560 low-noise preamplifier) before a lock-in amplifier (SRS SR810) demodulates the frequency modulation of the FIR radiation using 2f detection at 100 kHz. In the earlier work on the 81.8 cm^{-1} band, gated boxcars were used to integrate the signal before downloading into a 486-PC. The 28.0 cm^{-1} band was recorded using the new signal processing method, wherein the signal is averaged by a digital storage oscilloscope (Tektronix TDS320) and then downloaded.

The pulsed molecular beam is produced by expanding either pure Ar or 70% Ne in He, saturated with D_2O, through a 101.6-mm-long slit. Nozzle backing pressures in the range of 1 to 2 atm were employed. At a pulse repetition rate of 43 Hz the vacuum chamber was maintained at a pressure of approximately 40 mTorr by a Roots blower (Edwards EH4200) backed by two rotary pumps (Edwards E2M275).

B. 28.0 cm^{-1} band

We report the observation of a VRT spectrum for $(D_2O)_3$ at 28.0 cm^{-1} [0.839 186 8(3) THz], the lowest frequency intermolecular vibration observed in a water cluster to date. A total of 137 rovibrational transitions were recorded in a 5 cm^{-1} region. The spectrum, depicted in Fig. 3(a), has the appearance of a symmetric rotor perpendicular band. Figure 3(b) shows three transitions from the $|K|=3\leftarrow 2$ Q branch. The most intense transitions were observed in the R branch with signal-to-noise ratios up to 100:1. Although Doppler-limited linewidths (full width at half-maximum) of 0.9 MHz were obtained, the frequency uncertainty of each line is 2 MHz, arising from the uncertainty in the output frequency of the FIR laser.

The manifestation of bifurcation tunneling in the water trimer, which is not included in the effective torsional Hamiltonian, is readily apparent in Fig. 3(b), wherein each rovibrational transition is split into a quartet. The observed quartet intensity ratios (approximately 1:5:10:7) are consistent with the group theoretical (G_{48}) nuclear spin statistics[7] of 11:54:108:76, and the spacings between each of the four lines is 0.9 MHz. However, anomalous quartet intensity patterns were observed for the $|K|=0\leftarrow 1$ P-, Q-, and R-branch transitions, with approximate intensity ratios of 2:9:4:6 as shown in Fig. 4(a). For these quartets the individual lines exhibit an uneven spacing with a small J dependence. Similar anomalous quartets were observed in the $|K|=0\leftarrow 1$ transitions in the 98.1 cm^{-1} $(D_2O)_3$ band.[7] Such effects have been explained by van der Avoird *et al.*[23,24] in terms of bifurcation tunneling (also called donor tunneling) and Coriolis coupling associated with the torsional motions.

From the most recent torsional model[23,24] the $k=\pm 2^l\leftarrow 0$ transition was predicted to occur at either 17.2 or 25.2 cm^{-1}, depending on which *ab initio* potential energy surface was employed in the calculation. Furthermore, prior to this work only three low frequency (<40 cm^{-1}) torsional transitions in $(D_2O)_3$ were unobserved. Consequently the 28.0 cm^{-1} band was assumed to arise from the $k=\pm 2^l\leftarrow 0$ transition; the results of the spectroscopic fit presented below show this assumption to be correct. A summary of the characteristics of this band are presented in Table II.

C. 81.8 cm^{-1} band

The 81.8 cm^{-1} [2.453 571 6(7) THz] VRT spectrum of $(D_2O)_3$ was first recorded[8] in 1993, but was subsequently remeasured at higher sensitivity following the development of the pulsed slit jet assembly.[38] A total of 111 rovibrational

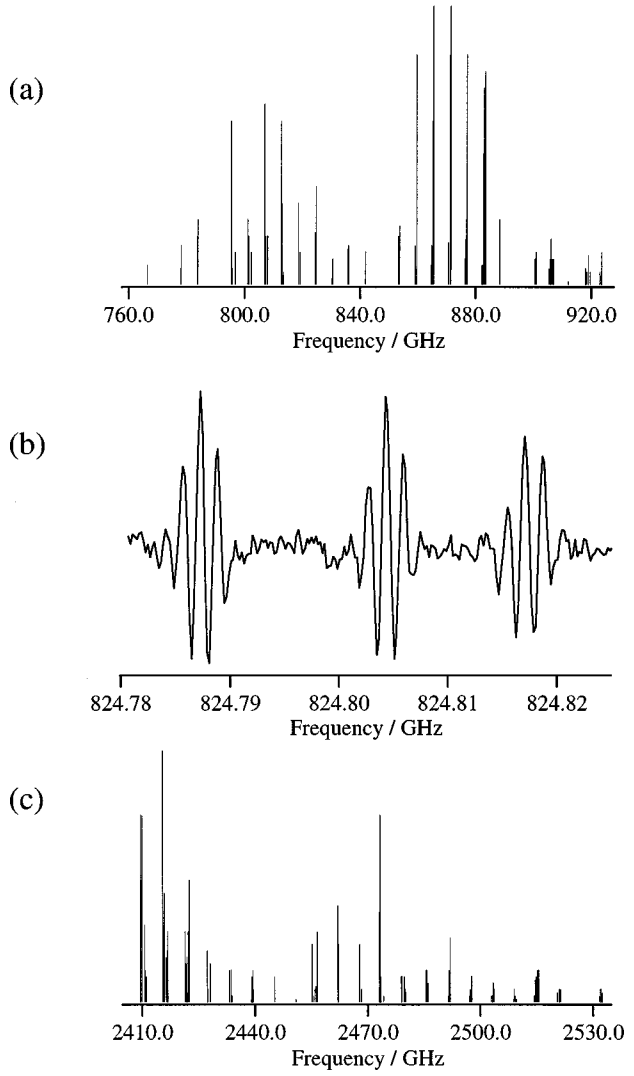

FIG. 3. (a) A stick spectrum of the 28.0 cm^{-1} [0.839 186 81 (3) THz] perpendicular VRT band of $(D_2O)_3$ which has been assigned to the $k=\pm 2^l \leftarrow 0$ torsional transition. The most intense *R*-branch lines have a signal-to-noise ratio of 100 : 1. (b) An experimental recording of the $|K|=3\leftarrow 2$ *Q* branch in the 28.0 cm^{-1} band, with each transition split into a ''normal'' quartet as a result of bifurcation tunneling. (c) A stick spectrum of the 81.8 cm^{-1} [2.453 571 (1) THz] perpendicular VRT band, assigned to the $k=3^u \leftarrow 1^l$ torsional transition. This band is much less intense, with a maximum signal to noise ratio of only 20 : 1, partly because it originates from the first excited torsional state.

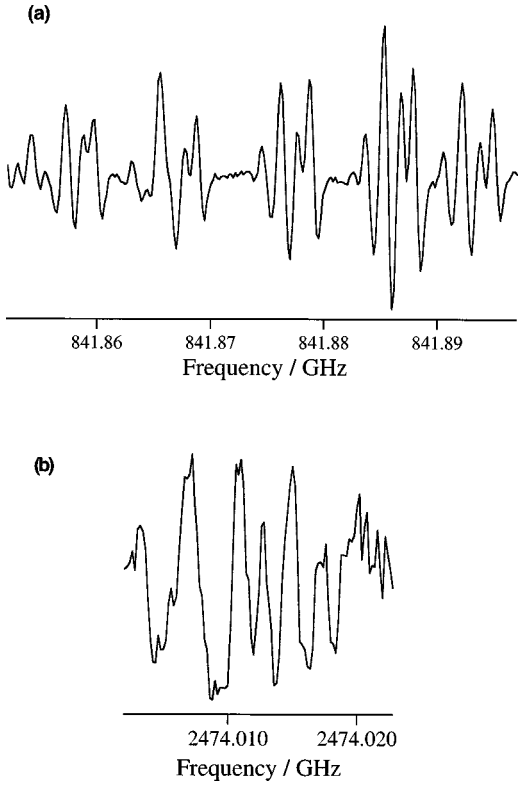

FIG. 4. ''Anomalous'' bifurcation tunneling quartet patterns observed for the $|K|=0\leftarrow 1$ rovibrational transitions of (a) the 28.0 cm^{-1} band (intensity ratio 2 : 9 : 4 : 6), and (b) the 81.8 cm^{-1} band (intensity ratio 5 : 3 : 5 : 2).

transitions were observed, and these are reproduced in a stick spectrum in Fig. 3(c). Even at the higher sensitivity afforded by the pulsed source the maximum signal-to-noise ratio was only 20:1. Every rovibrational transition was split into a quartet as a result of bifurcation tunneling. Most quartets have a normal intensity pattern (7:10:5:1) and 2.7 MHz spacings between each of the lines. As before, anomalous quartet intensity patterns were observed for the $|K|=0\leftarrow 1$ transitions, with approximate intensity ratios of 5:3:5:2; note that these quartets had signal-to-noise ratios of only 5:1 as shown in Fig. 4(b). This spectrum has been assigned to the $k=3^u \leftarrow \pm 1^l$ torsional transition by several theoretical calculations.[22,24,40] A summary of the details for this band can be found in Table II.

V. ANALYSIS AND RESULTS

A. Summary of previous studies

Several theoretical studies of the torsional (or pseudorotation) dynamics in the water trimer have been reported, ranging in sophistication from one-dimensional,[20] two-dimensional[21] and three-dimensional (3D)[22] calculations, up to the recent work by van der Avoird *et al.* which also includes overall rotation of the cluster[23,24] as well as bifurcation tunneling. The basic conclusions reached by these studies have been consistent; because the potential barrier to the deuteron ''flipping'' motion is calculated to lie below the 3D zero-point energy level for $(D_2O)_3$, the resulting ''tunneling splittings'' are very large. Although the pattern of energy levels in the torsional manifold is the same for all the theoretical studies, the actual calculated energies are

TABLE II. Summary of the principal characteristics of the five torsional transitions observed in $(D_2O)_3$.

Transition frequency / cm^{-1}	Band type	Torsional assignment	Relative intensity	References
28.0	Perpendicular	$k=\pm 2^l \leftarrow 0$	5.0	This work
41.1	Parallel	$k=3^l \leftarrow 0$	125.0	9,10
81.8	Perpendicular	$k=3^u \leftarrow \pm 1^l$	1.0	This work
89.6	Parallel	$k=\pm 2^u \leftarrow \pm 1^l$	1.5	2
98.1	Perpendicular	$k=\pm 2^u \leftarrow 0$	5.0	7

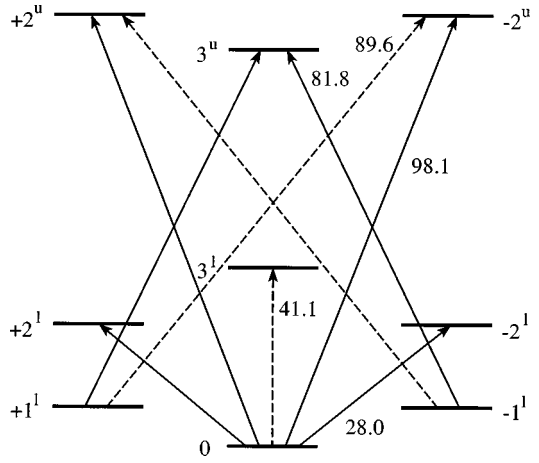

FIG. 5. The torsional energy level manifold for $(D_2O)_3$, showing the nine lowest levels labeled with the k quantum number. The solid arrows represent the six observed perpendicular ($\Delta K=\pm 1$) subbands, the three observed parallel subbands ($\Delta K=0$) are shown as dashed arrows. The transition frequencies (in cm^{-1}) for each band are also indicated.

very dependent on the level of theory as well as the torsional potential energy surface[18,19] employed in the calculations.

A generalized torsional energy level manifold for $(D_2O)_3$, including all the observed transitions, is shown in Fig. 5. From group theory, the torsional selection rule can be shown to be[7,23,41]

$$-k'+k''+K'-K''=3\ (\text{modulo}\ 6), \tag{14}$$

where k is the torsional quantum number. From this expression, the allowed transitions can be determined. For example, the $k=3^l\leftarrow 0$ torsional transition corresponds to a single parallel type band ($\Delta K=0$). The $k=\pm 2^l\leftarrow 0$ transition actually corresponds to two perpendicular type subbands, viz. the $k=+2^l\leftarrow 0$ transition must obey a $\Delta K=-1$ selection rule, and the $k=-2^l\leftarrow 0$ transition must obey $\Delta K=+1$. The implications of these selection rules are critical to the correct assignment of the $(D_2O)_3$ VRT spectra, which are most appropriately considered to comprise nine subbands rather than the five bands listed in Sec. I. The status of the 28.0, 41.1, 81.8, 89.6, and 98.1 cm^{-1} VRT bands, prior to the global fit, is discussed below and summarized in Table II; note that the relative band intensities were crudely estimated from the best signal-to-noise ratios, and do not take into account the different FIR laser line powers and detectors used.

The first rotationally resolved spectrum of $(D_2O)_3$ was the 89.6 cm^{-1} band observed by Pugliano and Saykally[2,8] in 1992. Although clearly of parallel type, the spectrum exhibited far too many transitions to be accounted for by a single well-behaved band. This led to the assumption that the spectrum arose from an asymmetric rotor and thus exhibited asymmetry doublets. The corresponding analysis did not account for the strongly perturbed spectrum particularly well. In light of the theory in Secs. II and III, it is now evident that the observed spectrum consists of two parallel subbands, the $k=-2^u\leftarrow +1^l$ and $k=+2^u\leftarrow -1^l$ torsional transitions, both obeying $\Delta K=0$. Recently Cruzan[42] obtained rotational assignments for the two subbands using the combination differences method. However, no satisfactory fit of the 89.6 cm^{-1} band had been achieved prior to this work.

Originally observed in 1993, the 81.8 cm^{-1} VRT band has long evaded a detailed analysis. This strongly perturbed spectrum is of perpendicular type. It thus consists of two subbands, the $k=3^u\leftarrow +1^l$ transition ($\Delta K=-1$) and the $k=3^u\leftarrow -1^l$ transition ($\Delta K=+1$). Although a partial rotational assignment was recently obtained,[42] attempts to fit this band have failed. The 41.1 cm^{-1} parallel band, assigned to the $k=3^l\leftarrow 0$ torsional transition ($\Delta K=0$), was first reported by Suzuki and Blake[9] in 1994. We recently rescanned the spectrum at the much higher sensitivity afforded by the pulsed slit valve assembly, allowing several new rovibrational transitions to be recorded. The spectrum has now been assigned and fit using an oblate symmetric rotor energy expression; as before, no perturbations or anomalous bifurcation tunneling quartets were observed.[10]

The 98.1 cm^{-1} perpendicular band was both observed and analyzed in detail by Liu *et al.*[7] in 1994. The spectrum is fully assigned, and most of the transitions fit using an oblate symmetric rotor energy expression. However, a Coriolis-type perturbation to the $|K|=1\leftarrow 0$ rovibrational transitions was not discussed until recently.[42] This spectrum also consists of two subbands resulting from the $k=+2^u\leftarrow 0$ ($\Delta K=-1$) and $k=-2^u\leftarrow 0$ ($\Delta K=+1$) transitions. The most recently observed $(D_2O)_3$ VRT band, at 28.0 cm^{-1}, is described above. It has the appearance of a perpendicular symmetric rotor spectrum, and has been assigned to the $k=+2^l\leftarrow 0$ ($\Delta K=-1$) and $k=-2^l\leftarrow 0$ ($\Delta K=+1$) torsional transitions. The global fit of the entire $(D_2O)_3$ VRT data set is given below. Table III summarizes the optimized parameters (torsional energies, rotational and distortion constants, and Coriolis parameters) obtained from the final fit.

B. The global fit

1. 41.1 cm^{-1} band

The 41.1 cm^{-1} parallel band was chosen as the logical starting point for the global fit since it can be described precisely by the oblate symmetric rotor energy level expression

$$E_{J,K}=E_0+BJ(J+1)+(C-B)K^2-D_JJ^2(J+1)^2 -D_{JK}J(J+1)K^2-D_KK^4, \tag{15}$$

where E_0 is the vibrational energy of state (k,n), B and C are its rotational constants, and D_J, D_{JK} and D_K are quartic distortion constants. This expression holds for the nondegenerate torsional levels with $k=0$ and $k=3$, cf. Eq. (8). The quartic terms were added to account for the higher than second-order perturbation effects which are not considered in Sec. II. Because a $\Delta K=0$ oblate top spectrum does not allow the independent determination of both C rotational constants, only the difference between the upper and lower state C constants could be determined. Aside from this, the parameters obtained from the fit describe the $k=0$ and $k=3^l$ levels extremely well for the rovibrational levels sampled, with K ranging from 0 to 11, and J from 0 to 11. With a total of 87 transitions included in the fit the rms of the residuals was <1 MHz, well within the experimental uncertainty of 2 MHz.

TABLE III. Optimized parameters (in MHz, except for ζ which is dimensionless) from the global fit of 554 rovibrational transitions assigned to the torsional manifold of the fully deuterated water trimer. The parameters A, B, C, D_J, D_{JK}, and D_K are the standard symmetric top rotational and distortion constants. The Coriolis coupling parameters ζ and μ_{++} are explained in the text. The C rotational constant for the $k=0$ torsional state could not be fit without correlation and so was fixed at the correlated value.

(k,n)	0^l	$+1^l$	-1^l	$+2^l$	-2^l	3^l	3^u	$+2^u$	-2^u
E_0	0.0[a]	255 976.49 (4)		839 186.81 (3)		1 232 139.43 (4)	2 709 548.14 (6)	2 940 936.95 (4)	
$B(=A)$	5796.34 (2)	5796.04 (3)		5794.64 (3)		5792.87 (3)	5788.73 (3)	5786.32 (2)	
C	3087.71[a]	3090.55 (5)		3095.79 (3)		3099.54 (2)	3089.97 (5)	3088.70 (2)	
D_J	0.0293 (3)	0.0297 (4)	0.0288 (4)	0.0271 (4)	0.0261 (4)	0.0265 (5)	0.0286 (5)	0.0278 (4)	0.0285 (4)
D_{JK}	−0.042 (1)	−0.050 (1)	−0.050 (1)	−0.044 (1)	−0.039 (2)	−0.045 (1)	−0.044 (1)	−0.048 (1)	−0.041 (1)
D_K	0.016 (2)	0.023 (2)	0.028 (3)	0.020 (2)	0.016 (3)	0.022 (2)	0.021 (2)	0.027 (3)	0.014 (1)
ζ	0.0	−0.043 87 (2)		−0.048 19 (2)		0.0	0.0	0.000 31 (2)	
$\lvert\mu_{++}\rvert$	0.0	26.68 (1)		13.67 (3)		0.0	0.0	3.61 (1)	

[a]Value fixed to avoid correlation.

This band could be precisely fit to Eq. (15) due to the absence of Coriolis perturbations in the nondegenerate $k=0$ and $k=3^l$ levels.

2. 28.0 cm^{-1} band

Having accurately defined the torsional ground state (except for the value of C''), it was logical to extend the fit to include another band which originated from $k=0$. Accordingly the 28.0 cm^{-1} band, assigned as $k=\pm 2^l \leftarrow 0$, was selected. All rovibrational transitions involving $K'=0$ and 1 (in the $k=\pm 2^l$ states) were initially excluded from the fit because they were predicted to be perturbed by second-order Coriolis effects. Furthermore, to simplify the analysis, each of the two subbands comprising the spectrum was fit separately. We first attempted to fit each subband to the oblate symmetric rotor energy expression in Eq. (15). Although this yielded poor results, it did reveal an unexpected and large perturbation with a linear dependence on K'. This is clearly indicated in Fig. 6, which shows a plot of the sign and magnitude of this perturbation as a function of the K' quantum number; note that this effect must arise in the $k=\pm 2^l$ states because the $k=0$ state is known to be well-behaved from the assignment of the 41.1 cm^{-1} band. We originally modeled this perturbation using a first-order Coriolis term, which acts on the two otherwise degenerate $k=\pm 2^l$ states

$$H^{(1)}_{\text{Coriolis}} = \mp 2\zeta CK, \tag{16}$$

where ζ is a Coriolis constant. Such a first-order Coriolis effect was not expected, because it was shown in the paper by van der Avoird *et al.*[23] that the expectation value of the internal (vibrational) angular momentum generated by the torsional (pseudorotational) motion is zero. In Secs. II and III of the present paper, however, the origin of this linear Coriolis splitting is explained. It emerges directly from the torsional model of van der Avoird *et al.*[23] if one derives an effective rotational Hamiltonian, cf. Eq. (13), in which Coriolis coupling is taken into account through second order. Furthermore, it follows from the derivations in Sec. II that there is also a second-order Coriolis splitting of the states with $K=\pm 1$ and $k-K=3$, which is proportional to $J(J+1)$. This splitting originates from off-diagonal Coriolis coupling between the substates $k=+2^l$ and $k=-2^l$.

Having fit the two subbands independently, a combined fit was undertaken with a single $k=\pm 2^l \leftarrow 0$ band origin, a single set of rotational constants B and C, and a single linear Coriolis parameter ζ. We again included quartic distortion terms and, since the higher than second order perturbation effects are not included in the effective rotational Hamiltonian of Eq. (13), we allowed the quartic distortion con-

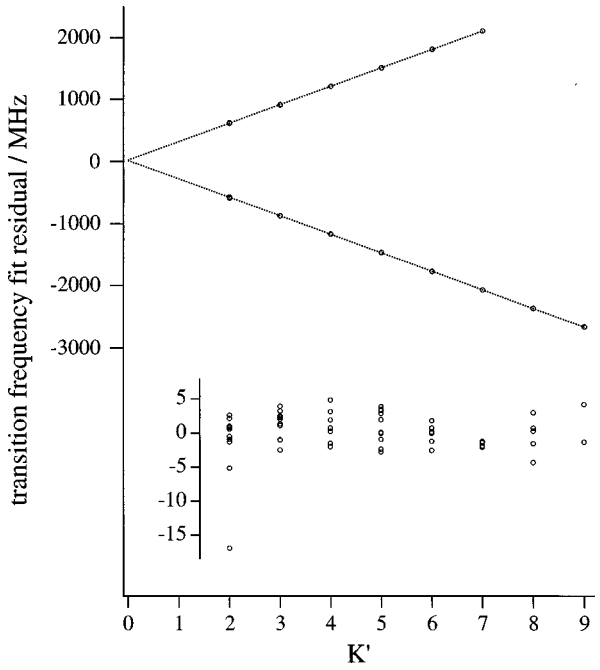

FIG. 6. A linear (first-order) Coriolis perturbation is evidenced by this graph of transition frequency residuals (MHz) for the 28.0 cm^{-1} band in the absence of Coriolis terms, plotted against K'. The large perturbation, depending linearly on K', changes the energy of the $k=-2$ levels by $+2\zeta CK'$ and the energy of the $k=+2$ levels by $-2\zeta CK'$. Both sets of data were fit to straight lines, and the scatter of the data points about these lines is highlighted in the inset graph which displays a greatly expanded scale. Note that the two data points with the largest scatter (-5 and -17 MHz) correspond to transitions involving $K'=2$ and high J'. These errors are largest because at this stage of the fit the effects of the off-diagonal second-order Coriolis coupling had not been included.

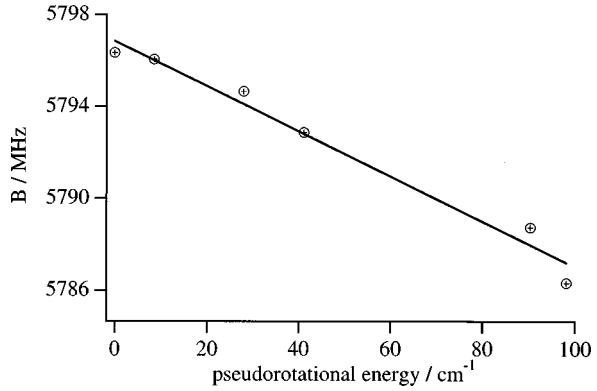

FIG. 7. A plot of the rotational constants (B) for the nine energy levels investigated in $(D_2O)_3$ vs torsional energy. The value of the rotational constants decreases almost linearly as a function of increasing torsional energy. Such an effect could be rationalized as resulting from a gradual 0.003 Å increase in the oxygen–oxygen separation from the lowest to the highest torsional levels observed.

stants D_J, D_{JK}, and D_K to be different for the two subbands. The subbands, containing 122 transitions, merged perfectly and the final fit yielded a rms residual of approximately 1 MHz. The values of the quartic distortion constants D_J, D_{JK}, and D_K for the two subbands turn out to be rather similar, cf. the parameters in Table III. For the $k=+2^l$ state, rovibrational levels were sampled with K' ranging from 0 to 7, and J' from 1 to 10. However, as a consequence of the $\Delta K=+1$ selection rule, the $K'=0$ manifold of levels was not sampled in the $k=-2^l$ state; only transitions to levels with K' ranging from 1 to 9, and J' ranging from 1 to 11 were observed.

3. 98.1 cm^{-1} band

The only other VRT band to originate from the torsional ground state, centered at 98.1 cm^{-1}, is assigned to $k=\pm 2^u \leftarrow 0$. With $k=0$ very well defined, including this as the third band in the global fit seemed a logical approach. A total of 68 transitions for both subbands were observed and added to the fit, with J' ranging from 1 to 8 and K' from 0 to 8. The Coriolis perturbations for this band were smaller than they were for any of the other transitions involving degenerate levels. The linear Coriolis splitting is essentially nonexistent and the off-diagonal second-order Coriolis perturbation is a factor of 4 smaller than in the $k=\pm 2^l$ levels, which is what permitted Liu *et al.*[7] to obtain a reasonable fit without including Coriolis perturbations.

4. 89.6 cm^{-1} band

Having accurately defined the $k=\pm 2^u$ states we turned our attention to the 89.6 cm^{-1} spectrum, assigned to the $k=-2^u \leftarrow +1^l$ and $k=+2^u \leftarrow -1^l$ torsional transitions. The initial fit included both forms of the Coriolis perturbation described for the other bands. The resulting fit was good, although it was the worst of the four bands currently included in the global analysis. This perhaps indicates that extremely small third and higher order perturbations should technically be included in this band. The resulting errors (rms residual $\approx$1.5 MHz), however, were still smaller than our experimental precision of 2.0 MHz. The final fit of the 89.6 cm^{-1} spectrum included 172 transitions, with J' (for $k=+2^u$) ranging from 1 to 16, and J' (for $k=-2^u$) ranging from 1 to 13.

5. 81.8 cm^{-1} band

The 81.8 cm^{-1} band was the last to be included in the global fit, and was assigned as the $k=3^u \leftarrow \pm 1^l$ torsional transition. With the parameters for the perturbed $k=\pm 1^l$ lower states previously determined, the fit of the 81.8 cm^{-1} band proceeded under the following assumption. The singly degenerate $k=3^u$ excited state was assumed to be unperturbed because, from the 41.1 cm^{-1} band, this was shown to be the case for both the singly degenerate $k=0$ and $k=3^l$ states. This assumption is also consistent with the model presented in Secs. II and III. A total of 101 rovibrational transitions were fit, with J' and K' (for $k=3^u$) ranging from 1 to 11 and 0 to 11, respectively. For the $k=+1^l$ state J'' and K'' ranged from 1 to 10 and 1 to 7, respectively. As before, the $\Delta K=-1$ selection rule does not allow transitions which originate from $K''=0$ levels. Hence, the J'' and K'' levels sampled in the $k=-1^l$ state ranged from 1 to 11 and 0 to 10, respectively.

6. Global fit

The final global fit included 554 rovibrational transitions from the nine measured $(D_2O)_3$ VRT subbands connecting nine torsional states. A total of 50 parameters were varied in the fit and the optimized parameters are presented in Table III. The largest correlation was 0.96, and most were below 0.5. The final rms deviation of the frequency residuals is 1.36 MHz, less than the experimental uncertainty of 2 MHz. It was noticed during the fit that transitions involving $|K|=1$ that are pushed to lower frequency by the linear Coriolis perturbation (an effect only observed in degenerate torsional levels) were split into two. This initially had the appearance of a further perturbation, and the $|K|=1$ transitions were thus left out of the fit until the very end. Attempts to fit the transitions involving these levels with the rotational constants ($A\neq B$) of an asymmetric rotor—since the breaking of the twofold $\pm K$ degeneracy was reminiscent of ''asymmetry doubling''—were unsatisfactory. An examination of the effective rotational Hamiltonian in Eq. (13), however, provides a natural explanation of this phenomenon. As it can be observed (for $J=2$) in Fig. 2, the matrix of this Hamiltonian for a doubly degenerate torsional level with $k=\pm 1$ or $k=\pm 2$ contains off-diagonal (second-order Coriolis) coupling elements between the $+k$ and $-k$ substates with different K, but the same values of $k-K$ (modulo 6). This lifts the twofold $\pm K$ degeneracy normally expected for symmetric rotors. The rotational states with $K=+1$ and $K=-1$ are coupled directly, for the $\pm|K|$ state with $|K|>1$ the coupling is indirect and, therefore, the splitting of these levels occurs in higher than second order and is extremely small. The relatively large (second-order) splitting of the $|K|=1$ levels manifests itself as an actual doubling in the spectra. Incorpo-

rating these splittings into the fit caused the previously highly correlated distortion parameters to become uncorrelated.

VI. DISCUSSION

One of the most interesting features of the global analysis presented above is that all of the perturbations in the spectra can be precisely explained by including Coriolis coupling between the internal (torsional) motions and the overall rotation through second order. For the explanation of this phenomenon we refer to the detailed model presented in Secs. II and III. We can also make a quantitative comparison between the calculated values of $2\zeta C$ and $|\mu_{++}|$, given in Sec. III, and the experimental values from the fit, listed in Table III. The values of $2\zeta C$ calculated from the model are too small by about a factor of 2, and the (very small) values of $|\mu_{++}|$ by about an order of magnitude. Apparently, the three-dimensional model for the torsional motions in the water trimer based on the *ab initio* potentials is not sufficiently accurate to achieve quantitative agreement with the measurements for these small Coriolis coupling parameters. The same conclusion was reached in Ref. 24. As was also stated in Ref. 24, the model yields rather good energies of the torsional levels, however. For the ''lower'' levels the best results were obtained with the van Duijneveldt-van de Rijdt and van Duijneveldt (DD) potential[19] and for the ''upper'' levels with the BGLK potential.[18]

From the rotational analyses of the nine measured VRT bands we are able to construct a graph of the *B* rotational constant for the energy levels as a function of torsional energy, see Fig. 7. Interestingly the rotational constants decrease by only 10 MHz over the energies sampled, and do so almost linearly with increasing torsional energy. An increase in torsional energy and hence in the rate of flipping could cause a small increase in the vibrationally averaged separation of the D_2O monomers. Using a simple structural model for the trimer,[10] an increase of only 0.003 Å in the average oxygen–oxygen distance, $R_{O\text{-}O}$, would explain the observed 10 MHz decrease in *B*. Such a small change vindicates the adiabatic separation of the torsional and hydrogen bond stretch/bend vibrational modes of the water trimer underlying the torsional model, the latter modes tending to change $R_{O\text{-}O}$ more drastically with increasing vibrational energy.

Having precisely determined the energies of the nine lowest lying torsional levels in $(D_2O)_3$ we are able to predict three additional low frequency (<100 cm^{-1}) transitions. Since only the $k=0$ and $\pm 1^l$ levels are believed to be populated in the ultracold slit jet expansion employed in our experiment, only transitions originating from these states can be observed at present. The first, a parallel band assigned to $k=3^u \leftarrow 0$ is predicted at 90.4 cm^{-1}. This frequency region was scanned but no $(D_2O)_3$ spectrum was observed. This result is not so surprising, however, since the transition is predicted to have a very small intensity.[21,43] The second band, assigned to $k=3^l \leftarrow \pm 1^l$, is predicted at 32.6 cm^{-1}. Although attempts to locate the spectrum failed, this can again be explained by the low intensity predicted for this transition.[21,43] The third and final band is predicted at 19.5 cm^{-1} and is assigned to the $k=\pm 2^l \leftarrow \pm 1^l$ transition. This frequency is close to the limit that the Berkeley spectrometers can practically attain, and was scanned several years ago without observing a water trimer spectrum. However, several experimental improvements have been instigated since then including the pulsed slit source, Herriott multipass optics, and the new detection and signal processing scheme. Thus, another attempt to locate this spectrum by rescanning close to 20 cm^{-1} would seem to be worthwhile, especially since this transition is predicted to be intense.[21,43] It would also be of high value to search for transitions at frequencies above 100 cm^{-1} and hence probe even higher lying torsional levels.

Whereas most of the low frequency torsional transitions have now been observed for $(D_2O)_3$, such is not the case for $(H_2O)_3$. The spectra of $(H_2O)_3$ are more complicated because of larger tunneling splittings associated with the lighter H atoms. For example, the line spacings within a bifurcation tunneling quartet increase from 1 to 5 MHz in $(D_2O)_3$ up to almost 300 MHz in $(H_2O)_3$. This is comparable to rotational spacings, and thus greatly increases the spectral complexity. A second consequence of the larger tunneling splittings is that the torsional energy levels in $(H_2O)_3$ are spaced approximately twice as far apart as in $(D_2O)_3$, and hence fewer low frequency transitions exist. Until recently, only a single VRT spectrum had been observed[7] in $(H_2O)_3$, at 87.1 cm^{-1}. This unperturbed symmetric top spectrum was correctly assigned to the $k=3^l \leftarrow 0$ torsional transition, and is equivalent to the 41.1 cm^{-1} band in $(D_2O)_3$. The first perpendicular band observed in $(H_2O)_3$, at 65.6 cm^{-1}, is currently under analysis.[44] It has been assigned to the $k=\pm 2^l \leftarrow 0$ torsional transition, and is equivalent to the 28.0 cm^{-1} band in $(D_2O)_3$. A third VRT spectrum of $(H_2O)_3$, centered near 43 cm^{-1}, is also under analysis[45] and is thought to arise from the $k=\pm 2^l \leftarrow \pm 1^l$ transition. The equivalent transition in $(D_2O)_3$, predicted at 19.5 cm^{-1}, has not yet been observed. This transition originates from the first excited state of $(H_2O)_3$ which lies approximately 23 cm^{-1} above the ground state and hence is not highly populated in the slit jet expansion. The observation of this transition will probably be facilitated by its large change in dipole moment.[43] Insights gained from the interpretation of the rovibrational structure of the $(D_2O)_3$ spectra will clearly aid in the analyses of these new $(H_2O)_3$ bands.

If the given assignments of the three $(H_2O)_3$ bands are correct, then the six lowest lying torsional levels in this cluster have been sampled. Consequently, a similar analysis as described in this paper for $(D_2O)_3$ should be possible for $(H_2O)_3$, which would thereby lead to the complete characterization of all the torsional energy levels up to 100 cm^{-1} in both $(H_2O)_3$ and $(D_2O)_3$. Finally, from the current band origins we are able to predict one additional low frequency transition in $(H_2O)_3$ at approximately 64 cm^{-1}, corresponding to $k=3^l \leftarrow \pm 1^l$. However, this transition is also predicted to have a very low intensity.[21,43]

To date, the highest dimensionality *ab initio* potential surfaces[18,19] describing the water trimer only include the three torsional angles of the free protons/deuterons. Model potentials—especially the (semi)empirical potentials used in simulations of liquid water—which describe all twelve inter-

molecular degrees of freedom are available, but the torsional frequencies in the trimer calculated from such potentials are very unrealistic.[46,47] From the present work, the energies of the nine lowest lying levels in $(D_2O)_3$ have been determined precisely. Furthermore, an equivalent understanding of the six lowest lying levels in $(H_2O)_3$ should soon be realized. With such precise and detailed experimental knowledge available it should now be possible to determine an improved potential energy surface for the water trimer, and in particular, to quantify the three-body forces that operate in this cluster. A major step toward this goal was very recently obtained by Fellers *et al.*, who obtained a six-dimensional pair potential of spectroscopic quality for the water dimer.[6] Such a pair potential could easily be applied to the trimer with the inclusion of an iterative induction term to account for the principal three-body interaction.[48–50] Theoretical work that involves the application of *ab initio* symmetry-adapted perturbation theory (SAPT) for the quantitative determination of the three-body interactions in the water trimer and larger clusters is also in progress.[51]

VII. CONCLUSIONS

We have reported a complete rovibrational analysis of the nine VRT subbands for the fully deuterated water trimer. This accounts for the entire data set currently existing for this cluster in the terahertz frequency regime. The quality of the fit is reflected by the rms of the frequency residuals of 1.36 MHz, which is even less than the typical experimental frequency precision of 2 MHz. This analysis required the development of a detailed three-dimensional model of the torsional motion in the water trimer. An examination of Coriolis coupling of the internal torsional motions to the overall rotation of the water cluster using the model Hamiltonian revealed strong perturbations. Remarkably, only second-order perturbation theory on this model system was required to fully explain our spectra, with the addition of empirical quartic distortion constants to reach experimental precision. Higher order perturbation theory was not required, nor was expanding the model Hamiltonian to include the other nine intermolecular degrees of freedom that describe this system. This suggests that extrapolation of this technique to larger clusters and higher energy systems is possible. The simultaneous fit of all existing VRT spectra serves both as a confirmation that the model describing the torsional energy level manifold presented in Fig. 5 is correct, and as confirmation of the specific torsional assignments.

ACKNOWLEDGMENTS

The authors thank Professor Herbert Strauss for helpful discussions, and Dr. Kun Liu and Don Lucas for assistance in scanning the 81.8 and 28.0 cm^{-1} spectra, respectively. R.J.S. thanks the Berkeley Miller Research Institute for support. Funding for this research was provided by the Experimental Physical Chemistry Program of the National Science Foundation (Grant No. CHE-9424482). R.J.S. and A.v.d.A. also wish to thank the NATO Collaborative Research Grants Program.

[1] K. L. Busarow, R. C. Cohen, G. A. Blake, K. B. Laughlin, Y. T. Lee, and R. J. Saykally, J. Chem. Phys. **90**, 3937 (1989).
[2] N. Pugliano and R. J. Saykally, Science **257**, 1937 (1992).
[3] J. D. Cruzan, L. B. Braly, K. Liu, M. G. Brown, J. G. Loeser, and R. J. Saykally, Science **271**, 59 (1996).
[4] K. Liu, M. G. Brown, J. D. Cruzan, and R. J. Saykally, Science **271**, 62 (1996).
[5] K. Liu, M. G. Brown, C. Carter, R. J. Saykally, J. K. Gregory, and D. C. Clary, Nature (London) **381**, 501 (1996).
[6] R. S. Fellers, L. B. Braly, M. G. Brown, and R. J. Saykally (unpublished).
[7] K. Liu, J. G. Loeser, M. J. Elrod, B. C. Host, J. A. Rzepiela, and R. J. Saykally, J. Am. Chem. Soc. **116**, 3507 (1994).
[8] K. Liu, M. J. Elrod, J. G. Loeser, J. D. Cruzan, N. Pugliano, M. G. Brown, J. Rzepiela, and R. J. Saykally, Faraday Discuss. **97**, 35 (1994).
[9] S. Suzuki and G. A. Blake, Chem. Phys. Lett. **229**, 499 (1994).
[10] M. R. Viant, J. D. Cruzan, D. D. Lucas, M. G. Brown, K. Liu, and R. J. Saykally, J. Phys. Chem. A **101**, 9032 (1997).
[11] K. Liu, M. G. Brown, M. R. Viant, J. D. Cruzan, and R. J. Saykally, Mol. Phys. **89**, 1373 (1996).
[12] J. D. Cruzan, M. R. Viant, M. G. Brown, and R. J. Saykally, J. Phys. Chem. A **101**, 9022 (1997).
[13] J. D. Cruzan, M. G. Brown, K. Liu, L. B. Braly, and R. J. Saykally, J. Chem. Phys. **105**, 6634 (1996).
[14] K. Liu, M. G. Brown, J. D. Cruzan, and R. J. Saykally, J. Phys. Chem. A **101**, 9011 (1997).
[15] J. D. Cruzan, M. R. Viant, M. G. Brown, D. D. Lucas, K. Liu, and R. J. Saykally, Chem. Phys. Lett. **292**, 667 (1998).
[16] K. Liu, M. G. Brown, and R. J. Saykally, J. Phys. Chem. A **101**, 8995 (1997).
[17] J. B. Hasted, S. K. Husain, F. A. M. Frescura, and J. R. Birch, Chem. Phys. Lett. **118**, 622 (1985).
[18] T. Bürgi, S. Graf, S. Leutwyler, and W. Klopper, J. Chem. Phys. **103**, 1077 (1995).
[19] J. G. C. M. van Duijneveldt-van de Rijdt, and F. B. van Duijneveldt, Chem. Phys. Lett. **237**, 560 (1995).
[20] M. Schütz, T. Bürgi, S. Leutwyler, and H. B. Bürgi, J. Chem. Phys. **99**, 5228 (1993); **100**, 1780(E)1994 ().
[21] W. Klopper and M. Schütz, Chem. Phys. Lett. **237**, 536 (1995).
[22] D. Sabo, Z. Bačić, T. Bürgi, and S. Leutwyler, Chem. Phys. Lett. **244**, 283 (1995).
[23] A. van der Avoird, E. H. T. Olthof, and P. E. S. Wormer, J. Chem. Phys. **105**, 8034 (1996).
[24] E. H. T. Olthof, A. van der Avoird, P. E. S. Wormer, K. Liu, and R. J. Saykally, J. Chem. Phys. **105**, 8051 (1996).
[25] S. S. Xantheas and T. H. Dunning, J. Chem. Phys. **99**, 8774 (1993).
[26] E. C. Kemble, *The Fundamental Principles of Quantum Mechanics* (McGraw-Hill, New York, 1937).
[27] L. C. Biedenharn and J. D. Louck, *Angular Momentum in Quantum Physics*, Encyclopedia of Mathematics Vol. 8 (Addison–Wesley, Reading, MA, 1981).
[28] D. Papoušek and M. R. Aliev, *Molecular-Vibrational-Rotational Spectra* (Elsevier, Amsterdam, 1982).
[29] R. N. Zare, *Angular Momentum* (Wiley, New York, 1988).
[30] D. R. Hershbach, J. Chem. Phys. **31**, 91 (1959).
[31] A. van der Avoird, J. Chem. Phys. **98**, 5327 (1993).
[32] E. Riedle and A. van der Avoird, J. Chem. Phys. **104**, 882 (1996).
[33] J. G. C. M. van Duijneveldt-van de Rijdt and F. B. van Duijneveldt (private communication).
[34] D. T. Colbert and W. H. Miller, J. Chem. Phys. **96**, 1982 (1992).
[35] G. C. Groenenboom and D. T. Colbert, J. Chem. Phys. **99**, 9681 (1993).
[36] G. A. Blake, K. B. Laughlin, R. C. Cohen, K. L. Busarow, D.-H. Gwo, C. A. Schmuttenmaer, D. W. Steyert, and R. J. Saykally, Rev. Sci. Instrum. **62**, 1693 (1991).
[37] G. A. Blake, K. B. Laughlin, R. C. Cohen, K. L. Busarow, D.-H. Gwo, C. A. Schmuttenmaer, D. W. Steyert, and R. J. Saykally, Rev. Sci. Instrum. **62**, 1701 (1991).
[38] K. Liu, R. S. Fellers, M. R. Viant, R. P. McLaughlin, M. G. Brown, and R. J. Saykally, Rev. Sci. Instrum. **67**, 410 (1996).
[39] D. R. Herriott, H. Kogelnik, and R. Kompfner, Appl. Opt. **3**, 523 (1964).
[40] W. Klopper, M. Schütz, H. P. Luthi, and S. Leutwyler, J. Chem. Phys. **103**, 1085 (1995).
[41] K. Liu, thesis, University of California at Berkeley, 1996.
[42] J. D. Cruzan, thesis, University of California at Berkeley, 1997.
[43] M. Geleijns and A. van der Avoird, J. Chem. Phys. **110**, 823 (1999).

[44] M. R. Viant, J. D. Cruzan, R. J. Saykally, M. Geleijns, and A. van der Avoird (unpublished).
[45] R. P. McLaughlin, R. J. Saykally, M. Geleijns, and A. van der Avoid (unpublished).
[46] D. J. Wales, J. Chem. Soc., Faraday Trans. **92**, 2505 (1996).
[47] D. J. Wales, in *Molecular Vibrations and Collision Dynamics*, edited by J. Bowman and Z. Bačić (in press).
[48] M. P. Hodges, A. J. Stone, and S. S. Xantheas, J. Phys. Chem. A **101**, 9163 (1997).
[49] J. K. Gregory and D. C. Clary, J. Chem. Phys. **102**, 7817 (1995).
[50] J. K. Gregory and D. C. Clary, J. Chem. Phys. **103**, 8924 (1995).
[51] R. Moszynski, A. Millet, P. E. S. Wormer, and A. van der Avoird (unpublished).